Chem. Senses 38: 541–550, 2013 doi:10.1093/chemse/bjt024

Ontogenetic Scaling of the Olfactory Antennae and Flicking Behavior of the Shore Crab, *Hemigrapsus oregonensis*

Lindsay D. Waldrop

Department of Integrative Biology, University of California, Berkeley, CA, USA and Department of Mathematics, University of North Carolina at Chapel Hill, CB#3420, Chapel Hill, NC, USA

Correspondence to be sent to: Lindsay D. Waldrop, Department of Mathematics, University of North Carolina at Chapel Hill, CB#3420, Chapel Hill, NC, USA. e-mail: lwaldrop@email.unc.edu

Accepted May 2, 2013

Abstract

Malacostracan crustaceans such as crabs flick antennae with arrays of olfactory sensilla called aesthetascs through the water to sense odors. Flicking by crabs consists of a quick downstroke, in which aesthetascs are deflected laterally (splayed), and a slower, reversed return stroke, in which aesthetascs clump together. This motion causes water to be flushed within and then held in between aesthetascs to deliver odor molecules to olfactory receptors. Although this odor sampling method relies on a narrow range of speeds, sizes, and specific arrangements of aesthetascs, most crabs dramatically change these during ontogeny. In this study, the morphometrics of the aesthetascs, array, and antennae and the flicking kinematics of the Oregon shore crab, *Hemigrapsus oregonensis* (Decapoda: Brachyura), are examined to determine their scaling relationships during ontogeny. The morphometrics of the array and antennae increase more slowly than would be predicted by isometry. Juvenile crabs' aesthetascs splay relatively further apart than adults, likely due to changing material properties of aesthetasc cuticle during growth. These results suggest that disproportionate growth and altered aesthetasc splay during flicking will mediate the size changes due to growth that would otherwise lead to a loss of function.

Key words: antennule, biofluid dynamics, decapoda, olfaction, ontogeny, sniffing

Introduction

Many crustaceans use dissolved chemical cues (odors) as a source of information throughout their ontogeny (Schmitt and Ache 1979; Dusenbery 1992; Atema 1995; Zimmer and Butman 2000). Larvae use olfactory cues to select a suitable habitat for settlement from the water column, to avoid predation, and to find food (Diaz et al. 1999; Pardieck et al 1999; Ferner et al. 2005; Lecchini et al. 2010). Adult crustaceans also rely on odors to locate food, to interact with conspecifics, and to mediate reproductive behaviors (Hazlett 1969; Caldwell 1979; Gleeson 1980; Gherardi et al. 2005; Atema and Steinbach 2007; Gherardi and Tricarico 2007; Shabani et al. 2009; Skog 2009).

A key aspect of olfaction is the process by which odor molecules are acquired by an organism. In order to use the information contained in odors, odor molecules must be captured from the surrounding environment (Moore et al. 1991b; reviewed in Koehl 2006). The act of odor capture is mediated by physical processes and, for many animals, is accomplished with a specialized chemosensory organ that intermittently samples the surrounding fluid.

Broadly, intermittent odor sampling, or "sniffing," is characterized by rapid fluid flow induced by an animal that provides a way to carry odor molecules to olfactory surfaces (Schmitt and Ache 1979). Intermittent sampling physically controls the flow of information from the environment to the olfactory system by introducing temporal structure to the delivery of odor molecules to sensory structures (Kepecs et al. 2006; Wachowiak 2011). Beyond simply delivering odor molecules to olfactory surfaces, there is evidence that sniffing plays a role in how olfactory information is encoded by olfactory neurons and ultimately perceived by animals, specifically to deal with confounding variables such as respiration and possibly environmental fluid flows (Schoenfeld 2006; Wachowiak 2011). Sniffing also creates unique spatiotemporal patterns of odors based on the distribution of odor molecules in a turbulent plume, which likely aids in orienting toward and tracking odor sources (Moore and Atema 1991; Moore et al. 1991a, b; Koehl et al. 2001; Keller et al. 2003).

Crustacean antennule design

Malacostracan crustaceans sniff by moving a specialized chemosensory organ (first antenna or antennule, Figure 1), studded with an array of long, flexible chemosensory sensilla (aesthetascs), through the water in a motion called "flicking" (Snow 1973; Schmitt and Ache 1979; Derby and Atema 1988). Aesthetascs are innervated with dendrites from chemosensory neurons; dendrites are separated by a thin layer of cuticle from the outside environment (Hallberg et al. 1997; Hallberg and Skog 2011). This layer of cuticle is permeable to several types of odorants and ions (Gleeson et al. 1996, 2000a, b,). Aesthetascs are arranged in rows with regular spacings between both aesthetascs and rows of aesthetascs on 1 branch of the biramous antennule.

For marine decapods, antennule flicking involves a rapid downstroke (Figure 2A) and slower return stroke (Figure 2B) in the opposite direction (Snow 1973; Koehl 2006). Like antennule morphology, the kinematics of flicking also vary between crustacean species. In crabs, the downstroke is about twice the speed of the return stroke. During the downstroke, the aesthetasc array is directly upstream and hydrodynamic drag causes the flexible aesthetascs to deflect laterally, increasing the distances between individual aesthetascs. The direction of the return stroke is reversed, causing the aesthetascs to be tightly clumped together (Snow 1973).

Fluid dynamics of sniffing

Odor molecules near the antennules are transported to the surfaces of the aesthetascs during flicking by a combination of molecular diffusion and water currents that are regulated by the interactions of water with the solid features of the

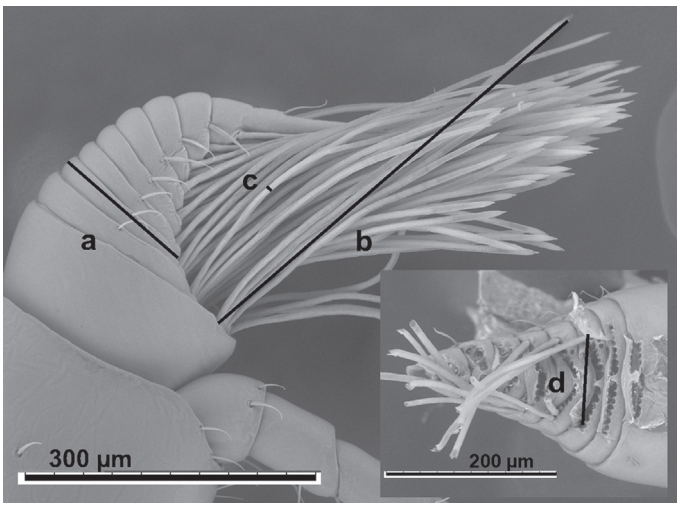

Figure 1 Scanning electron micrograph of side view of *H. oregonensis* antennule (inset: front view with aesthetascs removed) with morphometric measurements indicated by letters: (**a**) antennule side (thickness), (**b**) aesthetasc length, (**c**) aesthetasc diameter, and (**d**) array width.

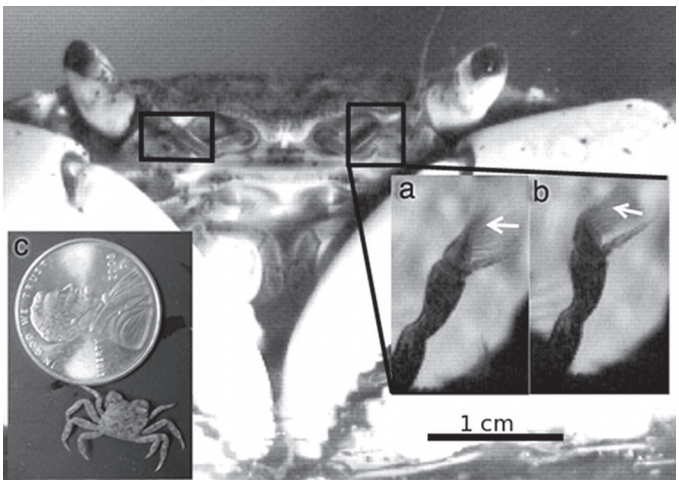

Figure 2 Anterior view of adult *H. oregonensis*. Antennules are enclosed by black boxes. (**a**) Close-up view of antennule during downstroke of flick showing aesthetascs (marked by white arrow) spread apart; (**b**) close-up view of antennule during return stroke of flick, showing aesthetascs (marked by white arrow) clumped together; (**c**) juvenile *H. oregonensis* individual with penny for scale.

array (Atema 1995; Goldman and Patek 2002; Reidenbach et al. 2008; reviewed in Koehl 2006). During antennule movement, a thin layer of water adheres to the solid surfaces of the aesthetascs ("no-slip" condition) and is sheared, creating a gradient of water velocities around each aesthetasc (boundary layer). The thickness of each boundary layer can be described as a function of the Reynolds number (Re):

$$\mathrm{Re} = \frac{Ud\rho}{\mu} \quad (1)$$

where U is the velocity relative to the aesthetascs, and d is the aesthetasc diameter, and μ and ρ are the dynamic viscosity and density of the fluid, respectively (Purcell 1977; Vogel 1994). Relative boundary layer thickness is proportional to $\mathrm{Re}^{-1/2}$; faster velocities result in thinner boundary layers and thicker boundary layers for slower velocities.

The fast movement (Re ~ 1) of the antennule during the downstroke creates thinner boundary layers between aesthetascs, allowing new water to flow in between the aesthetascs and displace water from previous flicks. Because aesthetascs are closer to their neighbors during the slower return stroke (Re ~ 0.1), the relatively thicker boundary layers around the aesthetascs interact, diverting water around the array and trapping a sample of water within the array (Koehl et al. 2001).

Each flick represents a discrete, intermittent sampling cycle or sniff as fluid is captured during the downstroke and then held against the chemosensory surfaces during the return stroke, akin to sniffing in other animals (Koehl 2006). This function reduces the boundary layers around each aesthetasc to allow more of the sensory surface to be exposed to new odor-containing fluid (Atema 1995; Koehl 2006). During the

time fluid is trapped in the array, odor molecules diffuse to the surfaces of each aesthetasc, enhancing the number of molecules captured per cycle (Stacey et al. 2002; Schuech et al. 2012).

Previous research on fluid flow within hair arrays shows that Re and other aspects of array design affect the amount of fluid that flows within an array (Cheer and Koehl 1987a; Loudon et al. 1994). Cheer and Koehl (1987a, b) developed models to describe fluid flow within a finite array of cylinders by measuring the fluid flowing through the array divided by possible flow in the absence of an array (leakiness). When Re increased between 0.01 and 1, the leakiness of an array increased disproportionately compared with increases in flow outside this Re range (Cheer and Koehl 1987a, b; Loudon et al. 1994). Small changes in the ratio of gap width between hairs to diameter of the hairs also had profound effects on array leakiness; larger ratios, or hairs spaced further apart, produced much leakier array than smaller ratios (Cheer and Koehl 1987a, b).

For many decapods, Res of antennule flicking fall within the range where small changes in speed and gap width are especially effective at changing fluid flow within the array. Deflection, or splay, of aesthetascs seen during the downstroke of brachyuran and anomuran crabs could also serve to increase flow within the array during the downstroke (Koehl 2011). Decreases in speed and gap width during the return stroke also decrease fluid flow within the array.

Scaling and the function of antennules

Many animals, including crustaceans, undergo a change in size during their lifetimes through growth. The Oregon shore crab, *Hemigrapsus oregonensis* grows from a 2-mm postsettlement juvenile to a 35-mm adult (Figure 2C). *Hemigrapsus oregonensis* juveniles share similar predation threats, conspecific interactions, and habitat preference as adults, suggesting that they have similar sensory ecologies (Hart 1935). The antennules of juveniles are absolutely much smaller than those of adult animals.

Having a much smaller body size, and by extension smaller antennule features, will result in lower Re during antennule flicking by decreasing the characteristic length d in equation (1). If juveniles' antennules were isometrically scaled compared with adults, crabs would begin life with antennules not capable of producing Re high enough to force fluid within the array during the downstroke (Re < 0.1), limiting the amount of their sensory surfaces able to access new odor samples. The aesthetasc arrays of juveniles would also have a smaller gap-width-to-diameter ratio, further exacerbating the effects of their small size on fluid flow through the array.

Allometric scaling of antennule features such as aesthetasc diameter and length could lessen the absolute change that these features experience during growth. If these features grow more slowly than expected by isometry, juvenile animals would have larger antennules both relative to their body size and larger on an absolute scale, possibly allowing the Re of the downstroke to remain in the range functionally important for sniffing (Mead and Koehl 2000).

Likewise, altered gap widths between aesthetascs during flicking could compensate for smaller aesthetasc features and still allow water to penetrate the array. How far aesthetascs splay depends on several variables: the relative proportions of aesthetasc structural features and material properties of aesthetasc cuticle. The distance an individual aesthetasc is deflected at its free end, D, can be modeled as a bending beam under a hydrodynamic drag force, F, distributed along the aesthetasc's length as follows:

$$D = \frac{FL^3}{8\mathrm{EI}} \tag{2}$$

where L is aesthetasc length, E is Young's modulus of aesthetasc chitin, and I is the second moment of area for a hollow tube (Wainwright et al. 1982; Vogel 2003). Young's modulus is a measure of a material's stiffness, describing the relationship between stress and strain. I, which describes the distribution of material that would resist bending, for a hollow tube is:

$$I = \frac{\pi}{4}\left(R_\mathrm{i}^4 - R_\mathrm{o}^4\right) \tag{3}$$

where R_o is the outer radius and R_i is the inner radius of the aesthetasc.

An important part of equation (2) is the flexural stiffness of the aesthetasc, EI, which represents both its structure through I, the second moment of area, and its material properties represented by Young's modulus, E. Either the material properties (changes in E) or the structure through allometric scaling (changes in I) could vary during ontogeny to produce altered splay ratios.

Because the ability to sniff, or intermittently sample odors, by crustaceans depends heavily on the morphology of the antennule and kinematics of flicking, predictions can be formed regarding the ability of juvenile crabs to discretely sample odors by examining changes in antennules during ontogeny. In this study, I investigate the changes in morphological and structural characteristics of antennules and kinematics of antennule flicking likely to impact sniffing during the ontogeny of the Oregon shore crab, *H. oregonensis*. It is likely that due to allometric growth of the antennules, juvenile crabs will continue to operate within the sensitive Re shared by other crustaceans despite a large change in body size during growth. Additionally, increasing the splay ratio of juvenile crabs would result in leakier arrays during the downstroke of flicking due to a change in either the structural or the material properties of the aesthetascs.

Materials and methods

Collection and maintenance of animals

Hemigrapsus oregonensis intermolt individuals were collected from the shore during low tide on the Emeryville shoreline of the San Francisco Bay, CA, USA. Animals were grouped according to size and kept in containers of seawater with aeration at 12 °C. Animals were supplied with macro and micro algae and frozen shrimp.

The carapace width (used as an index of body size) of each animal was measured to the nearest 0.1 mm at the widest point (between the third distal carapace teeth) with standard digital calipers. Adult animals were sexed according to the shape of the abdomen, but small juvenile animals were not sexed due to insufficient differences in external anatomy. After kinematic observations were made, animals were relaxed in 14% $MgCl_2$ in isotonic seawater (Lincoln and Sheals 1979). Both antennules were removed with forceps.

Scanning electron microscopy

Antennules were taken from *H. oregonensis* individuals and photographed using scanning electron microscopy (SEM). Specimens of whole antennules from each crab were fixed for an hour in 2% glutaraldehyde in 0.1 M sodium cacodylate buffer, pH 7.2. Antennules were then postfixed in 1% osmium tetroxide for 1 h and washed with the sodium cacodylate buffer (Mead et al. 1999). The aesthetascs of an antennule from each crab were then removed with a scalpel, whereas the second antennule from each crab was left with intact aesthetascs. Specimens were then dehydrated in an alcohol series and dried in a Critical Point Dryer (Tousimis AutoSamdri 815). Micrographs of the aesthetasc-bearing segments of the antennules were taken using a Hitachi TM-1000 Environmental Scanning Electron Microscope with a 15 kV beam at various magnifications.

Morphometrics

Measurements of aesthetascs diameter, aesthetasc cuticle thickness, aesthetasc length, and array width at the third segment were taken from SEMs (see Figure 1 for measurements) using *ImageJ* (Abramoff et al. 2004) to the nearest 10^{-2} µm. Antennule size was measured as the distal length of the third aesthetasc-bearing segment from the base of the antennule in 2 linear dimensions: the antennule thickness and the array width. Each measurement represents either a single measurement where only one measurement could be taken (antennule thickness and array width) or the average of 3 to 5 measurements on different aesthetascs of the same individual where multiple measurements could be taken (aesthetasc diameter, aesthetasc length, and aesthetasc cuticle thickness).

The growth rate of each morphometric measurement was compared against the increase in carapace width (body size). The natural log of morphometric measurements for individual animal was plotted against the natural log of carapace width, and regressions were calculated using the least-squares method of linear regression in the OpenOffice.org statistical package. The resulting slopes (uncertainty given as the standard error, s_e) were used to test for isometry where line slope would equal 1. All measurements of length are expected to be proportional to carapace width, and the null hypothesis of isometry is a slope (β_0) of 1 (H_0: $\beta = \beta_0$). Slopes not equal to 1 indicate allometric growth (H_a: $\beta \neq \beta_0$).

To test the difference between the slopes of each regression against the expected slope, the standard method of testing the results of a linear regression against a presumed slope was used (Devore 1987; Dodds et al. 2001). The t value is calculated based on the assumption that 2 linearly related variables exhibiting normal distributions would differ at least by as much as the expected and actual slopes (β_0 and β) vary:

$$t = \frac{\beta - \beta_0}{s_e} \quad (4)$$

P values are then calculated from a student's bimodal t-distribution with $(n - 2)$ degrees of freedom at $\alpha = 0.05$.

Kinematics

Antennule flicking by crabs was captured on video to analyze their movement. Crabs were starved for 2 to 3 days so they would be responsive to odors during filming. An individual crab's carapace widths were measured and then the crab was placed in a small container of still seawater and allowed to acclimate for 15 min before filming. The container had a millimeter scale and was surrounded by a temperature bath. The size of the container limited animal movement but was large enough not to interfere with antennule movement. Animals smaller than 8 mm in carapace width were glued to a small wooden dowel to limit movement and held in a small dish under a Wild Heerbrugg dissecting microscope with a scale micrometer. The field was illuminated by fiber optic light sources (Cole Parmer 9741–50) to minimize heating of the water bath. The temperature was monitored and held between 12 °C and 14 °C during filming. Shrimp extract was prepared by placing several grams of frozen shrimp in 250 mL of water for half an hour and straining off the liquid. To illicit flicking behavior, a small amount of shrimp extract was dripped into the water. Flicking motions were captured with a RedLake MotionScope PCI 1000s camera (Redlake Inc.) at 1000 frames per second.

Selected clips, those showing antennule flicking in the focal plane of the camera, were then digitized with Graphclick (Arizona Software Inc.) and calibrated with a millimeter scale bar (large animals) or stage micrometer (small animals) located in each video clip. The antennule tip and bases of aesthetasc array were digitized in each frame throughout the flicking event. Distances between positions from consecutive

frames were divided by the time step between frames and compared to find the peak velocities, and the sum of distances measured in each frame was divided by the total time to find mean velocities. Out of several video clips, 3 to 5 flicking events were digitized per animal, and average mean and peak velocities were calculated for each of the downstroke and return stroke movements for every animal.

To estimate the distance between the aesthetascs of the array during flicking, 2 splay ratios were calculated per animal. The edges of the aesthetasc array were selected in Graphclick by taking single frames of the antennule where the splay was greatest during the downstroke. The distances between the tips and bases of the aesthetascs were calculated from digitized positions. The distances of tips of the aesthetascs were divided by the length of the array base to find the splay ratio. Two splay ratios were calculated from 2 orientations: the side view (antennule flicking parallel to the focal plane) and front view (antennule flicking normal to the focal plane). Values represent the average of 2 to 5 measurements per individual crab. The downstroke and return velocities were used to calculate Res using a kinematic viscosity of seawater (1.20×10^{-6} m^2 s^{-1}) at 30‰ and 15 °C (Vogel 1994).

Results

Antennule morphology

Figure 3 plots select features, and Table 1 summarizes measurements of morphological features and reports results of natural log plots (slopes, y intercepts, correlation coefficients, and confidence intervals). All features measured in Table 1 had slopes that differed significantly from the slope expected for isometry ($m = 1$). For the size range in this study (3.9–27 mm), the antennules of the smallest juveniles are 87 µm wide and increase to 240 µm by adulthood. Aesthetasc lengths vary during growth from 347 to 648 µm, and aesthetasc diameters vary from 5.69 to 8.1 µm. During growth, antennules also add aesthetasc-bearing segments to their antennules, from 6 segments in juveniles to 11 in adults, increasing the total number of aesthetascs from 87 to 172. These differences from the expected slopes indicate that both antennules and the aesthetasc arrays scale much more slowly, giving small juveniles much larger antennules and aesthetascs relative to carapace width than large adults.

Variables affecting the gap width between aesthetascs are array width, aesthetasc diameter and length, and cuticle thickness. Aesthetasc diameter affects gap-width-to-diameter ratio and Re, the 2 major factors in the velocity of fluid flow through a aesthetasc array. Aesthetasc diameter scales with carapace width more slowly than all other measurements, changing by a factor of less than 1.5, whereas carapace width increases by a factor of 7. Aesthetasc length and cuticle thickness also affect the deflection of the aesthetascs. The aesthetasc lengths of small animals are considerably longer relative to their carapace width, and their aesthetascs are disproportionately thick, suggesting that deflection of the aesthetasc during the downstroke and, therefore, the splay ratio remain similar over all carapace widths.

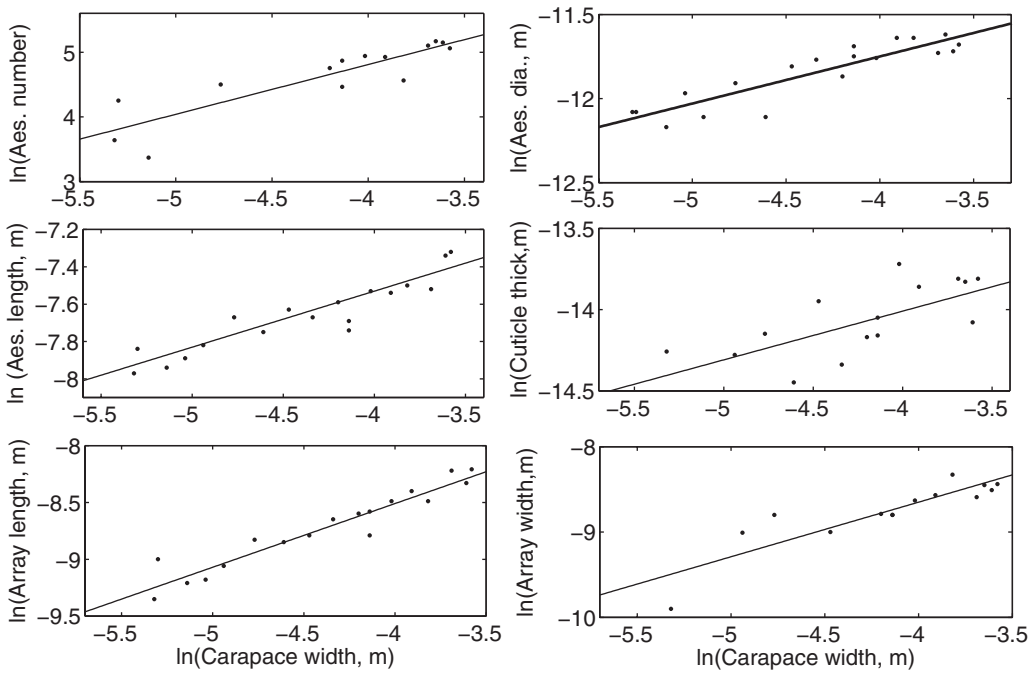

Figure 3 Select morphometric features measured versus natural log carapace width plots. Top left, number of aesthetascs; top right, aesthetasc diameter; middle left, aesthetasc length; middle right, aesthetasc cuticle thickness; bottom left, aesthetasc array length; bottom right, aesthetasc array width.

Table 1 Summary of sample size (n), regression slopes (± standard error, s_e), correlation coefficients (r^2), y intercepts, 95% confidence intervals for slope, and significance for 7 measured features

Variable	n	Slope ± s_e	r^2	y Intercept	P (slope = 1)	95% Confidence
Antennule thickness	18	0.56 ± 0.04	0.91	-6.27 ± 0.19	<0.0000001	0.44–0.68
Aesthetasc array						
Width	14	0.64 ± 0.1	0.78	–6.10 ± 0.41	<0.0001	0.94–0.34
Length	12	0.54 ± 0.09	0.79	–5.92 ± 0.39	<0.00002	0.27–0.81
Aesthetascs						
Diameter	19	0.28 ± 0.03	0.81	–10.6 ± 0.15	<0.0000001	0.18–0.38
Length	18	0.30 ± 0.03	0.86	–6.36 ± 0.13	<0.0000001	0.20–0.40
Cuticle thickness	15	0.30 ± 0.09	0.48	–12.8 ± 0.37	<0.00001	0.04–0.56
Hair number	14	0.77 ± 0.12	0.78	7.89 ± 0.27	0.2	0.67–0.87

Flicking kinematics

Table 2 contains a summary of kinematic values (downstroke and return velocities and durations). Figure 4 shows kinematic values plotted as a function of carapace width. Across the size range, average downstroke velocities range from 3.8 to 14.5 cm s^{-1}, and average return stroke velocities range from 1.38 to 7.82 cm s^{-1}. Duration of the downstroke and return stroke range from 8.0 to 14 ms and 16 to 43 ms, respectively. Downstroke and return stroke durations have no relationship with carapace width, maintaining a constant value throughout ontogeny.

Res of downstroke and return strokes were calculated using aesthetasc diameters and mean downstroke and return velocities (Table 2) and plotted against carapace width as shown in Figure 4. Re ranged from 0.27 to 1.17 during the downstroke, and return stroke Res ranged between 0.12 and 0.65. All Res remain in the sensitive range of $0.1 \leq Re \leq 10$. There are significant positive relationships between Re and carapace width for both the downstroke ($n = 13$, $P = 10^{-4}$) and return stroke ($n = 13$, $P = 7 \times 10^{-3}$).

Aesthetasc splay

The measured splay ratios of the downstroke, representing gap width, are reported in Table 2 and plotted against carapace width as shown in Figure 4. Side and front splay ratios range from 1.56 to 2.99 and 2.00 to 4.35 across the carapace width range, respectively. However, both splay ratios have a small, negative slope when plotted against carapace width, indicating that splay ratios are relatively larger for smaller animals. These slopes are both significantly different from a slope of zero (see Table 2 for statistics). For small juveniles, increased splay ratios coupled with fewer aesthetascs per unit array width would increase the gap-width-to-diameter

Table 2 Summary of sample size (n), regression slopes (± standard error, s_e), correlation coefficients (r^2), y intercepts, 95% confidence intervals for slope, and significance for kinematic parameters and Re for single-log transformed plots.

Variable	n	Slope ± s_e	r^2	y Intercept	P	95% Confidence
Velocities						
Downstroke	13	0.51 ± 0.09	0.75	–0.08 ± 0.41	0.0001†	0.24 to 0.78
Return	13	0.70 ± 0.1	0.83	–0.03 ± 0.44	0.007†	0.41 to 0.99
Duration						
Downstroke	13	$(1.7 \pm 0.7) \times 10^{-3}$	0.33	0.02 ± 0.003	0.04*	$(-0.3 \text{ to } 3.7) \times 10^{-3}$
Return	13	$(1.3 \pm 3) \times 10^{-3}$	0.02	0.03 ± 0.01	0.63*	$(-6.7 \text{ to } 8.3) \times 10^{-3}$
Mean Re						
Downstroke	9	0.46 ± 0.08	0.82	0.42 ± 0.21	0.00009†	0.21 to 0.71
Return	9	0.30 ± 0.03	0.93	0.38 ± 0.08	0.000003†	0.21 to 0.40
Splay ratios						
Front	9	–0.77 ± 0.37	0.37	–0.26 ± 1.67	0.04*	–1.54 to 0.00
Side	8	–0.59 ± 0.19	0.62	–0.70 ± 0.84	0.01*	–1.18 to 0.59

*slope = 0; †slope = 1.

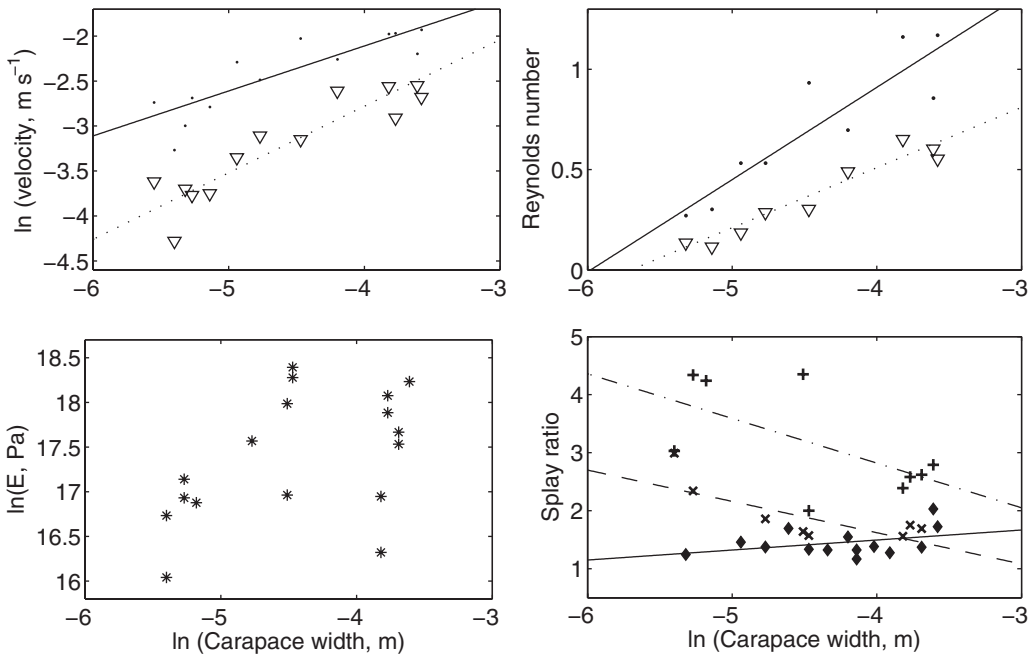

Figure 4 Select kinematic features plotted against natural log carapace width. Top left, downstroke (dots) and return (triangles) velocities; top right, downstroke (dots) and return (triangles) Res; bottom left, estimated Young's modulus, *E* (stars); bottom right, measured (front = +, side = x) and modeled (diamonds) splay ratios.

ratio, which would increase array leakiness for the range of Re seen during the downstroke.

Equations (2) and (3) provide a way to 1) model the splay ratios based on measured morphometrics and an assumed, constant Young's modulus, *E*, to compare them with measured values and 2) estimate the values of *E* during ontogeny based on measured splay ratios and morphometrics.

For part 1, equation (2) requires a hydrodynamic drag force on the aesthetascs. This force can be estimated by an equation for drag on a cylinder using the measured downstroke velocities, aesthetasc lengths and diameters, and cuticle thickness. I assumed that the hydrodynamic force, *F*, was distributed along the length of the aesthetasc and equal to

$$F = \frac{1}{2} C_D \rho d L U^2 \qquad (5)$$

(Lamb 1945) where C_D is the experimentally determined drag coefficient on a cylinder at intermediate Re (eq. 1) from the study by Finn (1953). The calculated deflection was based on equations (2), (3), and (5). Mean downstroke velocity was used for *U*, and the density of seawater at 30‰, 15 °C (1025 kg m^{-3}) was used for ρ (Vogel 1994). Each calculated deflection was then added to its corresponding array width measured from micrographs and divided by array width to find the modeled splay ratio. Young's modulus of cuticle was chosen as *E* = 137 MPa from the study by Taylor et al. (2007), representing the cuticle of a 1-h postmolt blue crab.

In Figure 4, modeled splay ratios for part 1 are compared with splay ratios measured from kinematics. Although measured splay ratios tend to decrease with increasing carapace width, the modeled splay ratios estimated from morphometrics increase with size. This dramatic difference between the slopes is significant ($n = 14$, $P < 10^{-5}$) and shows that the structure of the aesthetascs alone does not account for the observed relationship between measured splay ratio and carapace width.

For part 2, the measured splay ratios and morphometric data were used to estimate real values of Young's modulus *E* using equation (2). Figure 4 shows results of the Young's modulus estimation. Calculated *E* ranged from 9.25 to 97.3 MPa, showing an increase in *E* during growth by an order of magnitude. The slope of the regression representing change in *E* during ontogeny is significantly different from zero ($n = 17$, $P = 0.03$), the expected slope if no change in *E* occurred.

Discussion

Scaling relationships of array morphology and kinematics

Crustaceans, including brachyuran crabs, intermittently and discretely sample odors (sniff) by altering the kinematics of antennule flicking to increase fluid flow within their aesthetasc arrays during the downstroke and limit fluid flow within their arrays during the return stroke. Intermittent odor sampling occurs in this way only when antennule

morphology and flicking kinematics are restricted to a certain range of Res (eq. 1), in which small changes in antennule velocity, aesthetasc diameter, or gap widths between aesthetascs lead to dramatic effects on the fluid flow in an aesthetasc array (Koehl 2006). In order for juvenile Oregon shore crabs to fall within this range, the antennules of juvenile crabs would need to operate in the transitional Re range despite their considerably smaller body size.

The allometric scaling of morphological and kinematic features of *H. oregonensis* antennules supports this prediction. Aesthetasc diameter and length and array width number all increase much more slowly than predicted by isometry. These structures' slower rates of growth during ontogeny also slows the change in Re of the aesthetasc array and will potentially increase array leakiness compared with isometric arrays. In combination with flicking kinematics, the Re of the smallest juveniles was Re > 0.10. Despite the antennules of juvenile crabs operating at much lower Re than adults, they stay within the sensitive range in which dramatic shifts in fluid flow could still occur.

Scaling of aesthetasc deflection

Measured from kinematic data, the relationship between aesthetasc splay during the downstroke and carapace width supports the hypothesis that small juveniles have relatively larger splay ratios compared with adult animals. Along with fewer total aesthetascs, larger splay ratios increase the gap width between aesthetascs in juvenile arrays during the downstroke. Because the Re of a small juvenile downstroke reaches only 0.27, not as high as the 1.2 seen as adults, this additional increase in gap-width-to-diameter ratio could increase the leakiness within the array that was lost by lower velocities during the downstroke and smaller size of the aesthetascs.

Using the morphometric and kinematic measurements of one of the smallest juvenile crabs studied (carapace width = 4.9 mm, aesthetasc diameter = 5.69 µm, array width = 50 µm, number of aesthetascs in row = 6, front splay ratio = 4.34), more precise predictions can be made regarding leakiness through the array during flicking using the model provided in the study by Cheer and Koehl (1987b). For a small crab, the calculated gap-width-to-aesthetasc-diameter ratio for 1 row of aesthetascs is about 30, which combined with the Re = 0.27 during the downstroke, falls within the high leakiness range (0.6–0.8) (Cheer and Koehl 1987b; Koehl 2006). During the return stroke, gap-width-to-aesthetasc-diameter ratio falls by 2 orders of magnitude to about 0.2, predicting very low leakiness (<0.2). These calculations suggest that the smallest crabs studied also have the necessary fluid dynamics to sniff. However, because the aesthetasc array is a more complicated 3-dimensional structure than the single line of hairs used in the Cheer and Koehl model, measurements of fluid flow within the array and estimates of odor molecule capture are necessary to confirm these predictions.

The model of aesthetasc deflection as a bending beam based on morphometric data and constant material properties showed the opposite trend with increasing carapace width as the measured splay ratio values (Figure 4). According to this model, splay ratios of small animals should be much smaller than adult animals and increase in value during growth. These results suggest that changes in the structural properties of the aesthetasc morphology (through the second moment of area I in eqs. (2) and (3)) do not sufficiently explain the relationship between splay ratio and carapace width.

When the beam-bending model is used in conjunction with the splay ratios measured through kinematics, it reveals a significant size-dependent relationship for the Young's modulus E of aesthetasc cuticle (Figure 4). These results indicate that the material properties of juvenile crab aesthetascs are different than those of the adults. Young's modulus of chitin has been shown to vary during the ontogeny of insects based on the functional use of the tissue and during ecdysis for brachyurans, making such changes for juvenile crabs possible (Vincent and Wegst 2004; Taylor et al. 2007). Having lower values of E as a juvenile would allow aesthetascs to deflect further with the same amount of applied force, producing greater splay ratios and a leakier array to capture odors during the downstroke.

Comparison to other crustacean species

Studies discrete odor sampling through a size range of the spiny lobster (*Panulirus argus*) and stomatopod (*Gonodactylus mutatus*) have shown that the antennule morphology and kinematics tend to maintain flicking aesthetasc Re within the transitional range where array leakiness is sensitive to small changes in velocity and gap width (Mead et al. 1999; Mead and Koehl 2000; Goldman and Koehl 2001). In these studies, the aesthetasc Re of *P. argus* was maintained over large changes in body size, whereas they increased in *G. mutatus* over growth. For shore crabs, aesthetasc Re increase but stay within the Re range in which small changes in velocity and gap width cause large changes in array leakiness.

Despite the significant differences between antennule and aesthetasc morphology, *H. oregonensis* individuals over a much larger body size range than previously studied show similar decrease in gap width between aesthetascs with increasing size. This effect seems to be accomplished by decreased values of E of aesthetasc cuticle in small juveniles animals, leading to relatively larger splay ratios, an effect not observed in other species of crustaceans.

Odor capture in environmental flows

Most environments in which crabs are found are characterized by the existence of steady or transient ambient currents, which could interfere with a crab's ability to capture odors discretely. Both *H. oregonensis* and the hermit crab *Pagurus*

alaskensis preferentially orients their antennules during flicking in ambient currents so that the aesthetasc array is directly upstream to any flow present in its surroundings (Snow 1973, personal observation). Preferentially orienting the antennule in this way results in the ambient currents adding to the speed of the downstroke, making the water speed relative to the antennule much higher than flicking in still water. This increase in speed (U) would also increase drag on the hairs (F) according to equation (5) and the Re of the downstroke according to equation (1), splaying the hairs further apart than in still water conditions and increasing gap-to-diameter ratio of the array. Theoretically, ambient flow would increase the amount of new fluid delivered around the aesthetascs during the downstroke. During the return stroke, the antennule's direction reverses and the ambient flow instead subtracts some of the speed of the return stroke with respect to the antennule. Slower velocities result in lower Re for the aesthetascs (eq. 1) and theoretically less fluid exchange within the array. Environmental flows would likely enhance odor sampling on the downstroke and limit escape of the sample during the return stroke.

Funding

This work was supported by the Virginia and Robert Gill Chair and a MacArthur Foundation Fellowship (to M. Koehl); a Sigma-Xi Grant-in-Aid of Research to the author; and by a Traineeship to the author (National Science Foundation Integrative Graduate Education and Research Traineeship [#DGE-0903711] to R. Full, M. Koehl, R. Dudley, and R. Fearing).

Acknowledgements

I thank M. Koehl for equipment, guidance, support, and critical reading of the manuscript; V. Rapp and P. Gursel for comments on manuscript; K. Dorgan for help in the field; G. Min and the UC Berkeley Electron Microscopy Lab; and the UC Berkeley Biomechanics group.

References

Abramoff MD, Magalhaes PJ, Ram SJ. 2004. Image processing with ImageJ. BioPhoto Intl. 11(7):36–42.

Atema J. 1995. Chemical signals in the marine environment: dispersal, detection, and temporal signal analysis. Proc Natl Acad Sci U S A. 92(1):62–66.

Atema J, Steinbach MA. 2007. Chemical communication and social behavior of the lobster Homarus americanus and other decapod crustacea. In: Duffy J, Thiel M, editors. Evolutionary ecology of social and sexual systems: crustaceans as model organisms. Oxford (NY): Oxford University Press. p. 115–144.

Caldwell RL. 1979. Cavity occupation and defensive behavior in the stomatopod gonodactylus-festai—evidence for chemically mediated individual recognition. Anim Behav. 27:194–201.

Cheer AYL, Koehl MAR. 1987a. Fluid-flow through filtering appendages of insects. IMA J Math Appl Med Biol. 4(3):185–199.

Cheer AYL and Koehl MAR. 1987b. Paddles and rakes—fluid-flow through bristled appendages of small organisms. J Theor Biol. 129(1):17–39.

Derby CD, Atema J. 1988. Chemoreceptor cells in aquatic invertebrates: peripheral mechanisms of chemical signal processing in decapod crustaceans. In: Atema J, Fay RR, Popper AN, Tavolga WN, editors. Sensory biology of aquatic animals. New York (NY): Springer-Verlag. p. 365–385.

Devore JL. 1987. Probability and statistics for engineering and the sciences. Monterey (CA): Brooks/Cole.

Diaz H, Orihuela B, Forward RB, Rittschof D. 1999. Orientation of blue crab, callinectes sapidus (rathbun), megalopae: responses to visual and chemical cues. J Exp Mar Biol Ecol. 233(1):25–40.

Dodds PS, Rothman DH, Weitz JS. 2001. Re-examination of the "3/4-law" of metabolism. J Theor Biol. 209(1):9–27.

Dusenbery DB. 1992. Sensory ecology: how organisms acquire and respond to information. New York (NY): W.H. Freeman.

Ferner MC, Smee DL, Chang YP. 2005. Cannibalistic crabs respond to the scent of injured conspecifics: danger or dinner? Mar Ecol Prog Ser. 300:193–200.

Finn RK. 1953. Determination of the drag on a cylinder at low Reynolds numbers. J Appl Phys. 24(6):771–773.

Gherardi F, Tricarico E. 2007. Can hermit crabs recognize social partners by odors? and why? Mar Freshwat Behav Physiol. 40(3):201–212.

Gherardi F, Tricarico E, Atema J. 2005. Unraveling the nature of individual recognition by odor in hermit crabs. J Chem Ecol. 31(12):2877–2896.

Gleeson RA. 1980. Pheromone communication in the reproductive-behavior of the blue-crab, Callinectes-sapidus. Mar Behav Physiol. 7(2):119–134.

Gleeson RA, Hammar K, Smith PJ. 2000a. Sustaining olfaction at low salinities: mapping ion flux associated with the olfactory sensilla of the blue crab Callinectes sapidus. J Exp Biol. 203(Pt 20):3145–3152.

Gleeson RA, McDowell LM, Aldrich HC. 1996. Structure of the aesthetasc (olfactory) sensilla of the blue crab, Callinectes sapidus: transformations as a function of salinity. Cell Tissue Res. 284(2):279–288.

Gleeson RA, McDowell LM, Aldrich HC, Hammar K, Smith PJ. 2000b. Sustaining olfaction at low salinities: evidence for a paracellular route of ion movement from the hemolymph to the sensillar lymph in the olfactory sensilla of the blue crab Callinectes sapidus. Cell Tissue Res. 301(3):423–431.

Goldman JA, Koehl MA. 2001. Fluid dynamic design of lobster olfactory organs: high speed kinematic analysis of antennule flicking by Panulirus argus. Chem Senses. 26(4):385–398.

Goldman JA, Patek SN. 2002. Two sniffing strategies in palinurid lobsters. J Exp Biol. 205(Pt 24):3891–3902.

Hallberg E, Johansson KUI, Wallen R. 1997. Olfactory sensilla in crustaceans: morphology, sexual dimorphism, and distribution patterns. Int J Insect Morphol Embryol. 26(3–4):173–180.

Hallberg E, Skog M. 2011. Chemosensory sensilla in crustaceans. In: Thiel M, editor. Chemical communication in Crustaceans. New York (NY): Springer. p. 103–121.

Hart JFL. 1935. The larval development of british columbia brachyura. I. xanthidae, pinnotheridae (in part) and grapsidae. Canadian Jour Res. 12(4):411–432.

Hazlett BA. 1969. "Individual" recognition and agonistic behaviour in Pagurus bernhardus. Nature. 222(5190):268–269.

Keller TA, Powell I, Weissburg MJ. 2003. Role of olfactory appendages in chemically mediated orientation of blue crabs. Mar Ecol Prog Ser. 261: 217–231.

Kepecs A, Uchida N, Mainen ZF. 2006. The sniff as a unit of olfactory processing. Chem Senses. 31(2):167–179.

Koehl MA. 2006. The fluid mechanics of arthropod sniffing in turbulent odor plumes. Chem Senses. 31(2):93–105.

Koehl, MAR. 2011. Hydrodynamics of sniffing by Crustaceans. In: Thiel, M, editor. Chemical communication in Crustaceans. New York (NY): Springer. p. 85–102.

Koehl MA, Koseff JR, Crimaldi JP, McCay MG, Cooper T, Wiley MB, Moore PA. 2001. Lobster sniffing: antennule design and hydrodynamic filtering of information in an odor plume. Science. 294(5548):1948–1951.

Lamb H. 1945. Hydrodynamics. New York (NY): Dover publications.

Lecchini D, Mills SC, Brie C, Maurin R, Banaigs B. 2010. Ecological determinants and sensory mechanisms in habitat selection of crustacean postlarvae. Behav Ecol. 21(3):599–607.

Lincoln RJ and Sheals JG. 1979. Invertebrate animals collection and preservation. Cambridge: Cambridge University Press.

Loudon C, Best B, Koehl M. 1994. When does motion relative to neighboring surfaces alter the flow through arrays of hairs? J Exp Biol. 193(1):233–254.

Mead KS, Koehl MA. 2000. Stomatopod antennule design: the asymmetry, sampling efficiency and ontogeny of olfactory flicking. J Exp Biol. 203(Pt 24):3795–3808.

Mead KS, Koehl MAR, O'Donnell MJ. 1999. Stomatopod sniffing: the scaling of chemosensory sensillae and flicking behavior with body size. J Exp Mar Biol Ecol. 241(2):235–261.

Moore PA, Atema J. 1991. Spatial information in the three-dimensional fine structure of an aquatic odor plume. Biol Bull. 181:408–418.

Moore PA, Atema J, Gerhardt GA. 1991a. Fluid-dynamics and microscale chemical movement in the chemosensory appendages of the lobster, homarus-americanus. Chem Senses. 16(6):663–674.

Moore PA, Scholz N, Atema J. 1991b. Chemical orientation of lobsters, Homarus americanus, in turbulent odor plumes. J Chem Ecol. 17(7):1293–1307.

Pardieck RA, Orth RJ, Diaz RJ, Lipcius RN. 1999. Ontogenetic changes in habitat use by postlarvae and young juveniles of the blue crab. Mar Ecol Prog Ser. 186:227–238.

Purcell EM. 1977. Life at low Reynolds number. Am J Phys. 45(1):3–11.

Reidenbach MA, George N, Koehl MA. 2008. Antennule morphology and flicking kinematics facilitate odor sampling by the spiny lobster, Panulirus argus. J Exp Biol. 211(Pt 17):2849–2858.

Schmitt BC, Ache BW. 1979. Olfaction: responses of a decapod crustacean are enhanced by flicking. Science. 205(4402):204–206.

Schoenfeld TA. 2006. Special issue: what's in a sniff?: the contributions of odorant sampling to olfaction. Chem Senses. 31(2):91–92.

Schuech R, Stacey MT, Barad MF, Koehl MA. 2012. Numerical simulations of odorant detection by biologically inspired sensor arrays. Bioinspir Biomim. 7(1):016001.

Shabani S, Kamio M, Derby CD. 2009. Spiny lobsters use urine-borne olfactory signaling and physical aggressive behaviors to influence social status of conspecifics. J Exp Biol. 212(Pt 15):2464–2474.

Skog M. 2009. Male but not female olfaction is crucial for intermolt mating in European lobsters (Homarus gammarus L.). Chem Senses. 34(2):159–169.

Snow PJ. 1973. Antennular activities of hermit crab, pagurus-alaskensis (benedict). J Exp Biol. 58(3):745–765.

Stacey MT, Mead KS, Koehl MA. 2002. Molecule capture by olfactory antennules: mantis shrimp. J Math Biol. 44(1):1–30.

Taylor JR, Hebrank J, Kier WM. 2007. Mechanical properties of the rigid and hydrostatic skeletons of molting blue crabs, Callinectes sapidus Rathbun. J Exp Biol. 210(Pt 24):4272–4278.

Vincent JF, Wegst UG. 2004. Design and mechanical properties of insect cuticle. Arthropod Struct Dev. 33(3):187–199.

Vogel S. 1994. Life in moving fluids: the physical biology of flow. 2nd ed. Princeton (NJ): Princeton University Press.

Vogel S. 2003. Comparative biomechanics: life's physical world. Princeton (NJ): Princeton University Press.

Wachowiak M. 2011. All in a sniff: olfaction as a model for active sensing. Neuron. 71(6):962–973.

Wainwright SA, Biggs WD, Currey JD, Gosline JM. 1982. Mechanical design in organisms. Princeton (NJ): Princeton University Press. Usa. Illus.Paper.

Zimmer RK, Butman CA. 2000. Chemical signaling processes in the marine environment. Biol Bull. 198(2):168–187.